Thermal (n, γ) cross section and resonance integral of ^{171}Tm

T. Heftrich,[1,*] M. Weigand,[1] Ch. E. Düllmann,[2,3,4] K. Eberhardt,[2] S. Fiebiger,[1] J. Glorius,[1,3] K. Göbel,[1] C. Guerrero,[5] R. Haas,[2,4] S. Heinitz,[6] J. Lerendegui-Marco,[5] F. Käppeler,[7] J. D. Kaiser,[1] U. Köster,[8] C. Langer,[1] S. Lohse,[2,4] F. Ludwig,[1] R. Reifarth,[1] D. Renisch,[2,4] K. Scheutwinkel,[1] D. Schumann,[6] N. Wiehl,[2,4] and C. Wolf[1]

[1]*Goethe University Frankfurt, Frankfurt am Main, Germany*
[2]*Johannes Gutenberg-Universität Mainz, Mainz, Germany*
[3]*GSI Helmholtzzentrum für Schwerionenforschung, Darmstadt, Germany*
[4]*HIM Helmholtz-Institut Mainz, Mainz, Germany*
[5]*Universidad de Sevilla, Sevilla, Spain*
[6]*Paul-Scherrer-Institut, Villigen, Switzerland*
[7]*Karlsruhe Institute of Technology, Germany*
[8]*Institut Laue-Langevin, Grenoble, France*

(Received 4 December 2018; published 27 June 2019)

Background: About 50% of the heavy elements are produced in stars during the slow neutron capture process. The analysis of branching points allows us to set constraints on the temperature and the neutron density in the interior of stars.
Purpose: The temperature dependence of the branch point ^{171}Tm is weak. Hence, the ^{171}Tm neutron capture cross section can be used to constrain the neutron density during the main component of the *s* process in thermally pulsing asymptotic giant branch (TP-AGB) stars.
Methods: A ^{171}Tm sample produced at the ILL was activated with thermal and epithermal neutrons at the TRIGA research reactor at the Johannes Gutenberg-Universität Mainz.
Results: The thermal neutron capture cross section and the resonance integral have been measured for the first time to be $\sigma_{\mathrm{th}} = 9.9 \pm 0.9$ b and $\sigma_{\mathrm{RI}} = 193 \pm 14$ b.
Conclusions: Based on our results, new estimations of the direct capture components' impact on the Maxwellian-nAveraged cross sections (MACS) are possible.

DOI: 10.1103/PhysRevC.99.065810

I. ASTROPHYSICAL SITES

Nearly all of the observed abundances of elements heavier than iron are formed by the *s* or the *r* process. The specific *s*-process path depends on temperatures and neutron densities in stars, neutron capture cross sections, and half-lives in case of unstable isotopes. Branch points are nuclei whose neutron capture rate and β-decay rate are of the same order of magnitude. The *s*-process path depends strongly on the neutron capture cross sections in these cases [1]. Branches are thus especially well suited to verify the *s*-process model.

The *s*-process path in the region of mass number $A = 171$ is depicted in Fig. 1 (grey arrows). It follows the stable erbium isotopes via neutron captures until it reaches the unstable ^{169}Er. Because of its short half-life (9.39 d) compared to the neutron capture time, under *s*-process conditions a β decay follows and produces the stable isotope ^{169}Tm. A subsequent neutron capture leads to the radioactive isotope ^{170}Tm with a half-life of 129 days, acting as branch point. According to [2], the half-life of ^{170}Tm does not change significantly below $kT \approx 30$ keV. Hence, this branch point can be used to constrain the neutron density during the main component *s* process. This means for the *s*-process path that either the neutron density is high enough to synthesize ^{171}Tm or β decay takes place and leads to the stable isotope ^{170}Yb. If the unstable ^{171}Tm is produced, it acts as a second branch point. Mostly depending on the neutron density, the unstable isotope ^{172}Tm (1.92 yr) is produced or it decays via β decay to the stable ^{171}Yb.

Therefore, the branch points ^{170}Tm and ^{171}Tm can be utilized to constrain the neutron density during the main component of the *s* process. An important step to achieve this is the investigation of the neutron capture cross sections of both isotopes. The focus of this work is on ^{171}Tm(n, γ). So far one activation experiment was performed with quasi-stellar neutrons of $kT = 25$ keV at Forschungszentrum Karlsruhe, Germany [3] and in 2015 a new activation experiment, at 40 keV, was performed at the LiLiT facility in SOREQ [4]. In 2014, a time-of-flight measurement was performed at the n_TOF facility at CERN [4]. The situation in the thermal region is very inconclusive. Reported data for the thermal neutron capture cross section ($kT = 25$ meV) range from 4 to 160 b [5,6]. This discrepancy is important because the direct capture (DC) component of the cross section yields

*t.heftrich@gsi.de

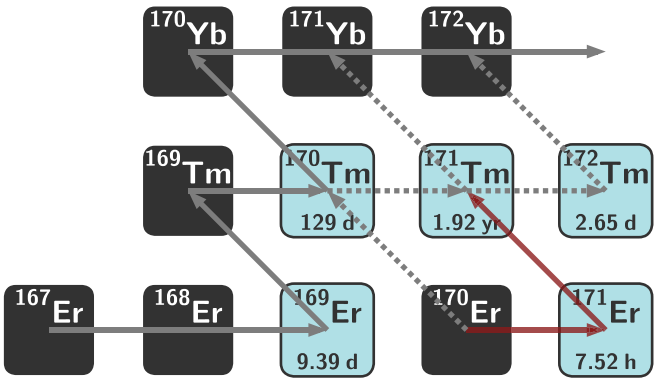

FIG. 1. The *s*-process reaction path between Er and Yb depicted by grey arrows. Secondary paths are represented by dashed lines. The radioactive isotopes ^{170}Tm and ^{171}Tm act as branch points and can be used to study the neutron density during the main component of the *s* process.

information for the extrapolation towards higher temperatures and the thermal cross section provides a constraint for the *s*-wave component of the DC cross section.

To obtain a reliable cross section in the keV regime, it was helpful to determine the largely unknown thermal neutron capture cross section of ^{171}Tm. An experiment was performed at the TRIGA type research reactor at the Institute of Nuclear Chemistry, Johannes Gutenberg-Universität, Mainz, Germany [7,8] via activation of an enriched ^{171}Tm sample.

II. THE ^{171}Tm ACTIVATION EXPERIMENT

The determination of the thermal neutron capture cross section of the branching point nucleus ^{171}Tm was performed at the TRIGA research reactor in Mainz via activation.

A. The radioactive ^{171}Tm sample

The radioactive ^{171}Tm sample was produced via irradiation of a ^{170}Er sample at the research reactor at ILL, Grenoble for 55 days. The resulting ^{171}Er nuclei decayed with a half-life of 7.52 hours to the isotope of interest, ^{171}Tm (Fig. 1). Afterwards, a chemical separation was performed at the Paul-Scherrer-Institut, Villigen, Switzerland [12]. The sample was characterized via spectroscopy of the 67 keV γ line of ^{171}Tm. The measurement was investigated by γ spectroscopy with a HPGe detector with a length of 67 mm and a diameter of 69 mm and a relative efficiency of 60%. The activity of the sample was determined by

$$A_{^{171}\mathrm{Tm}} = \lambda\left(\frac{C_\gamma}{\epsilon_\gamma I_\gamma f_\mathrm{m} f_\mathrm{dt}}\right), \qquad (1)$$

where the decay constant is $\lambda = \ln 2/t_{1/2}$, C_γ are the detected events, ϵ_γ the efficiency, I_γ the γ intensity of the emitted γ line, $f_\mathrm{m} = 1 - \exp(-\lambda_i t_\mathrm{m})$ the correction for the decay during the measurement, and f_dt is the correction for the deadtime of the detection system.

The efficiency calibration of the detector was performed with a calibrated solution of ^{60}Co, ^{85}Sr, ^{88}Y, ^{113}Sn, ^{137}Cs, ^{139}Ce, and ^{203}Hg, providing a wealth of γ lines over a broad energy range. The uncertainties of the source activities were 2.3%. For the γ intensity, a weighted average was done using two recent publications [10,11].

TABLE I. Parameters for the determination of the number of ^{171}Tm in the sample.

Parameter		Ref.
Half-life $t_{1/2}(^{171}\mathrm{Tm})$ (yr)	1.92±0.01	[9]
Events C_γ	30523 ± 180	
γ efficiency ϵ_γ (%)	0.213 ± 0.013	
γ intensity I_γ (%)	0.155 ± 0.005	[10,11]
Correction f_m (%)	<0.1	
Dead time f_dt (%)	<8	

On 20 March 2017, the number of ^{171}Tm nuclei was determined with the parameter given in Table I to

$$N_{^{171}\mathrm{Tm}} = (2.68 \pm 0.01_\mathrm{stat} \pm 0.09_\mathrm{sys}) \times 10^{15}, \qquad (2)$$

which corresponds about 50 MBq decay activity. Hence, the sample was measured at a large distance of 43.2 cm from the detector (Fig. 2). The dead time was in the order of 7%.

B. Determination of the neutron fluence

A typical reactor neutron spectrum is dominated by thermal neutrons with a Maxwell-Boltzmann energy distribution corresponding to $kT = 25.3$ meV. The epithermal neutron flux can be approximated with an energy dependence of $1/E$. The corresponding cross sections were disentangled by applying the cadmium-difference method, which requires two activations with largely different ratios of epithermal to thermal neutrons. Neutron monitors of Au, Sc, and Ta, which have well-known neutron cross sections, were used. The activities of the samples were determined using γ spectroscopy as described in Sec. II A. The number of activated nuclei was

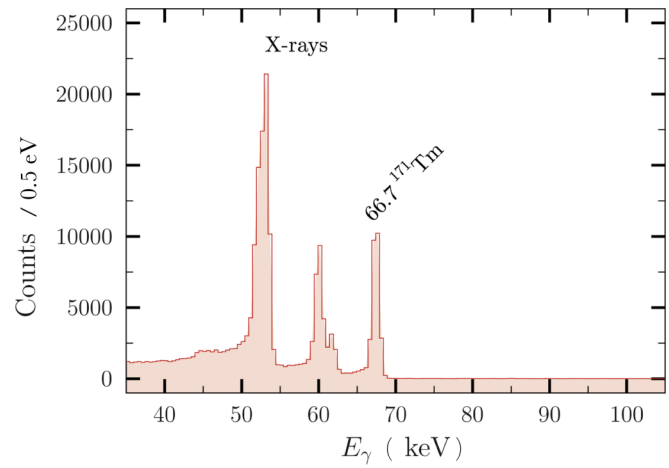

FIG. 2. Spectrum obtained for the ^{171}Tm sample characterization. Aside from the ^{171}Tm γ line at 66.7 keV, only x rays of the Tm isotopes are visible.

TABLE II. Decay characteristics and detection efficiencies of γ-ray emission of the investigated activated nuclei. Please note that the line intensity is the product of relative and absolute intensity: $I_\gamma = I_{\rm rel} I_{\rm abs}$.

Isotope	$t_{1/2}$ (d)	E_γ (keV)	$I_{\rm rel}$ (%)	$I_{\rm abs}$	Ref.	ϵ_γ (%)	$\sigma_{\rm th}$ (barn)[a]	$\sigma_{\rm RI}$ (barn)[a]
				Neutron monitors				
^{45}Sc	83.79 ± 0.04	889.277	99.984 ± 0.001	1	[13]	0.1191 ± 0.0011	27.2 ± 0.2	12.1 ± 0.5
		1120.545	99.987 ± 0.001			0.0999 ± 0.0010		
^{182}Ta	114.74 ± 0.12	1121.290	100	0.3524 ± 0.0008	[14]	0.0987 ± 0.0010	20.5 ± 0.5	655 ± 20
		1189.040	46.78 ± 0.11			0.09543 ± 0.0010		
		1221.395	77.27 ± 0.22			0.09346 ± 0.0010		
		1231.004	32.96 ± 0.08			0.09289 ± 0.0010		
^{198}Au	2.6941 ± 0.0002	411.80205	95.62 ± 0.06	1	[15]	0.2041 ± 0.0024	98.65 ± 0.09	1550 ± 28
				Tm sample				
^{172}Tm	2.65 ± 0.0125	1093.59	100 ± 5	0.060 ± 0.005	[16]	0.2809 ± 0.0030		
		1387.093	93 ± 5			0.2384 ± 0.0031		
		1465.86	75 ± 4			0.2294 ± 0.0032		
		1529.64	85 ± 5			0.2226 ± 0.0034		
		1608.37	69 ± 4			0.2149 ± 0.0035		

[a]All cross sections are adopted from [17].

calculated using

$$N(^{A+1}X) = \frac{C_\gamma}{\epsilon_\gamma I_\gamma f_{\rm a} f_{\rm w} f_{\rm m} f_{\rm dt}}, \tag{3}$$

where

$$f_{\rm a} = \frac{1 - \exp(-\lambda_i t_{\rm a})}{\lambda_i t_{\rm a}}, \tag{4}$$

$$f_{\rm w} = \exp(-\lambda_i t_{\rm w}), \tag{5}$$

$$f_{\rm m} = 1 - \exp(-\lambda_i t_{\rm m}) \tag{6}$$

are parameters to correct for the decay during the activation $f_{\rm a}$, the waiting time between activation and measurement $f_{\rm w}$, and the measurement $f_{\rm m}$. The small correction for the dead time of the detection system is represented by $f_{\rm dt}$. The involved parameters are listed in Table II). The resulting neutron fluences for both activations are listed in Table III.

TABLE III. Thermal and epithermal neutron fluence data for activations both with and without Cd shielding, respectively. The degree of activation of the monitors is given as activation ratio $R = N(^{A+1}X)/N(^{A}X)$.

Fluence without Cd	
R(Au) ($\times 10^{-7}$)	$1.74 \pm 0.03_{\rm stat} \pm 0.01_{\rm sys}$
R(Ta) ($\times 10^{-8}$)	$2.32 \pm 0.03_{\rm stat} \pm 0.02_{\rm sys}$
R(Sc) ($\times 10^{-8}$)	$6.87 \pm 0.12_{\rm stat} \pm 0.10_{\rm sys}$
$\Phi_{\rm th}$ ($\times 10^{14}$ cm^{-2})	$9.89 \pm 0.25_{\rm stat} \pm 0.20_{\rm sys}$
$\Phi_{\rm epi}$ ($\times 10^{13}$ cm^{-2})	$4.46 \pm 0.14_{\rm stat} \pm 0.14_{\rm sys}$
Fluence with Cd	
R(Au) ($\times 10^{-8}$)	$8.37 \pm 0.13_{\rm stat} \pm 0.01_{\rm sys}$
R(Ta) ($\times 10^{-10}$)	$7.52 \pm 0.09_{\rm stat} \pm 0.01_{\rm sys}$
R)(Sc) ($\times 10^{-8}$)	$4.24 \pm 0.07_{\rm stat} \pm 0.01_{\rm sys}$
$\Phi_{\rm th}$ ($\times 10^{14}$ cm^{-2})	$1.16 \pm 0.11_{\rm stat} \pm 0.15_{\rm sys}$
$\Phi_{\rm epi}$ ($\times 10^{13}$ cm^{-2})	$4.31 \pm 0.06_{\rm stat} \pm 0.11_{\rm sys}$

C. The activated Tm sample

The γ counting of the produced unstable ^{172}Tm nuclei was carried out with the same high-purity germanium detector as described in Sec. II A, including also the decay corrections. Above 1 MeV the five γ lines with the highest intensities were observed (Table II), but with a much lower count rate than the ^{171}Tm activity. In order to improve the signal-to-background ratio, we reduced the sample-detector distance to 13.2 cm and attenuated the low energy γ and x rays with a 2 mm thick lead sheet. The correction for the dead time was around 7%. Again, GEANT3 simulations revealed that cascade effects had no significant impact on the results. The number of the produced ^{172}Tm nuclei was determined according to Eq. (3).

D. Thermal (n, γ) cross section

The number of nuclei produced after the activation $N(^{A+1}X)$ can be expressed in terms of the thermal cross section $\sigma_{\rm th}$, the resonance integral $\sigma_{\rm RI} = \int_{E_{\rm cutoff}}^{2\ \rm MeV} \sigma(E)/E\, dE$ with the cutoff energy $E_{\rm cutoff} \approx 90$ meV, and the epithermal ($\Phi_{\rm epi}$) and thermal neutron fluences ($\Phi_{\rm th}$):

$$N(^{A+1}X) = N(^{A}X)(\Phi_{\rm th}\sigma_{\rm th} + \Phi_{\rm epi}\sigma_{\rm RI}), \tag{7}$$

where $N(^{A}X)$ is the number of target nuclei in the irradiated sample.

The cadmium difference method was used to disentangle the contributions from the thermal and epithermal neutrons. Two 10 minute irradiations were conducted using 1 mm Cd shielding in the first run and no shielding in the second one. Since the two irradiations were 43 days apart, the change of the number of ^{171}Tm nuclei in the sample during that time had to be taken into account. A spectrum of the activated sample is shown in Fig. 3. One finds

$$N_{172} = N_{171}(\Phi_{\rm th}\sigma_{\rm th} + \Phi_{\rm epi}\sigma_{\rm RI}), \tag{8}$$

$$N^{\bullet}_{172} = N^{\bullet}_{171}\left(\Phi^{\bullet}_{\rm th}\sigma_{\rm th} + \Phi^{\bullet}_{\rm epi}\sigma_{\rm RI}\right), \tag{9}$$

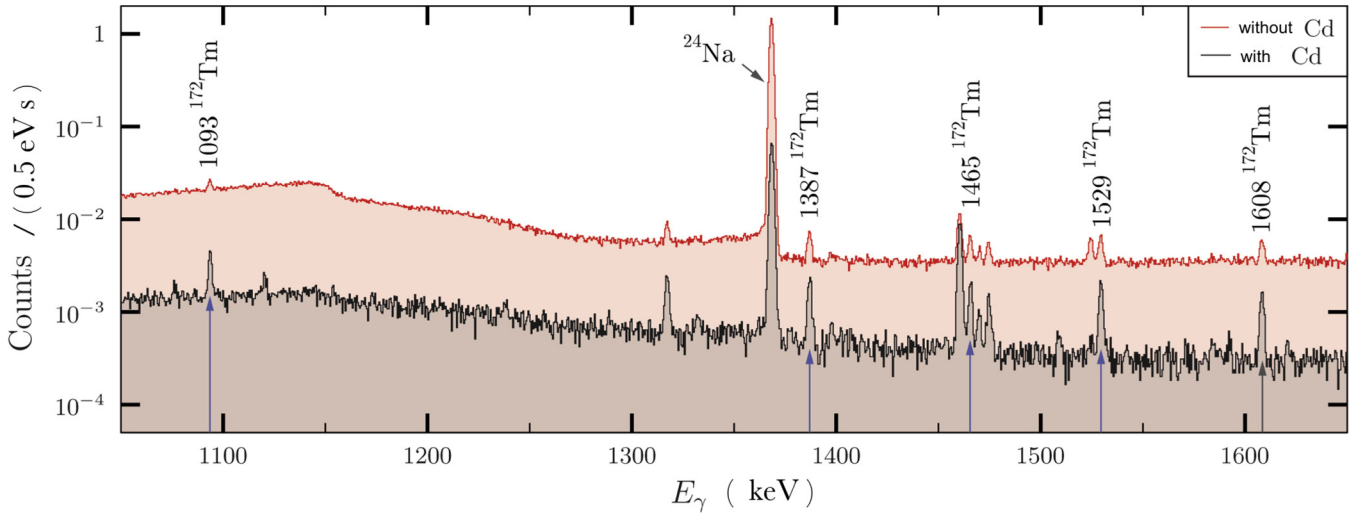

FIG. 3. γ-spectra from the ^{171}Tm sample after the activations with (black) and without (red) Cd shielding. ^{172}Tm lines are marked (blue arrows). Activated sodium was the major background source.

where $^\bullet$ denotes the use of the Cd shielding. Solving Eq. (8) for σ_{RI} gives

$$\sigma_{\mathrm{RI}} = \frac{N_{172}/N_{171} - \Phi_{\mathrm{th}}\sigma_{\mathrm{th}}}{\Phi_{\mathrm{epi}}}. \tag{10}$$

Together with Eq. (9) this leads to the expression for the thermal neutron capture cross section

$$\sigma_{\mathrm{th}} = \frac{N^\bullet_{172}N_{171}\Phi_{\mathrm{epi}} - N_{172}N^\bullet_{171}\Phi^\bullet_{\mathrm{epi}}}{N_{171}N^\bullet_{171}(\Phi^\bullet_{\mathrm{th}}\Phi_{\mathrm{epi}} - \Phi_{\mathrm{th}}\Phi^\bullet_{\mathrm{epi}})}. \tag{11}$$

The ratios of ^{171}Tm to ^{172}Tm are given in Table IV. For the ^{171}Tm(n,γ) reaction we obtained the thermal neutron capture cross section

$$\sigma_{\mathrm{th}} = (9.9 \pm 0.8_{\mathrm{stat}} \pm 0.3_{\mathrm{sys}})\ \mathrm{b} \tag{12}$$

and the resonance integral (RI)

$$\sigma_{\mathrm{RI}} = (193 \pm 12_{\mathrm{stat}} \pm 8_{\mathrm{sys}})\ \mathrm{b}. \tag{13}$$

E. Uncertainties

The systematic uncertainty for the flux determination is dominated by the γ efficiencies up to 1.6%, the decay intensities up to 0.3%, and the half-lives up to 0.1%. The errors resulting from the counting of the irradiated monitors are in the range of 0.6% to 2.4%.

The systematic uncertainties of the cross sections are dominated by those of the γ efficiencies up to 1.1%, the decay intensities up to 10.8%, and the half-lives up to 0.5%. The error induced by the γ counting of the samples is in the range of 4.9% to 10.8%. The main contributions to the uncertainties are listed in Table V.

TABLE IV. The numbers of ^{171}Tm and ^{172}Tm nuclei for both activations, with and without the Cd shielding.

Activation without Cd	
$N_{^{171}\mathrm{Tm}}$ ($\times 10^{15}$)	$2.68 \pm 0.01_{\mathrm{stat}} \pm 0.09_{\mathrm{sys}}$
$N_{^{172}\mathrm{Tm}}$ ($\times 10^{7}$)	$4.91 \pm 0.17_{\mathrm{stat}} \pm 0.02_{\mathrm{sys}}$
Activation with Cd	
$N_{^{171}\mathrm{Tm\text{-}Cd}}$ ($\times 10^{15}$)	$2.80 \pm 0.01_{\mathrm{stat}} \pm 0.09_{\mathrm{sys}}$
$N_{^{172}\mathrm{Tm\text{-}Cd}}$ ($\times 10^{7}$)	$2.64 \pm 0.17_{\mathrm{stat}} \pm 0.01_{\mathrm{sys}}$

III. SUMMARY AND DISCUSSION

To study the *s*-process reaction path, branch points are very important since they allow to constrain the conditions in the interior of stars [18,19]. The analysis of the interesting branch point ^{171}Tm is currently hampered by insufficient knowledge of the corresponding nuclear data. We report improved measurements of the thermal and resonance integral (RI) neutron capture cross sections of ^{171}Tm and the intensity of the 66.7 keV γ line.

TABLE V. All sources of uncertainties for the neutron capture cross section of ^{171}Tm. Most uncertainties are given as ranges, since, e.g., several γ lines with different uncertainties were analyzed.

Source of uncertainty	Uncertainty (%)
Neutron fluence determination	
Gamma intensities[a]	<0.3
Detection efficiency ϵ_γ[a]	[1.1, 1.6]
Factors f_{a}, f_{w} and f_{b}	<0.1
γ counting statistics[a]	[0.6, 2.4]
Cross section determination	
Gamma intensities[a]	[5.6, 10.8]
Detection efficiency ϵ_γ[a]	[0.9,1.1]
Factors f_{a}, f_{w} and f_{b}	<0.5
γ counting statistics[a]	[1.9,3.5]
Statistical uncertainty σ_{th}	14.1
Systematic uncertainty σ_{th}	2.2
Total uncertainty σ_{th}	14.3
Statistical uncertainty σ_{RI}	9.4
Systematic uncertainty σ_{RI}	8.3
Total uncertainty σ_{RI}	12.5

[a]Used for weighted averaging.

The thermal neutron capture cross section of ^{171}Tm was determined to be

$$\sigma_{\rm th} = (9.9 \pm 0.9)\ {\rm b} \tag{14}$$

Based on the cadmium-difference method, we found a resonance integral of

$$\sigma_{\rm RI} = (193 \pm 14)\ {\rm b} \tag{15}$$

Assuming a $1/v$ dependence of the cross section, one finds for the thermal cross section

$$\sigma_{\rm th} = \alpha \frac{1}{\sqrt{E_n = 25\ {\rm meV}}} \tag{16}$$

and for the resonance integral

$$\sigma_{\rm RI} = \int_{E_{\rm cutoff}}^{1\ {\rm MeV}} \frac{\sigma(E)}{E} dE. \tag{17}$$

The cutoff energy $E_{\rm cutoff}$ is the energy at which the thermal neutrons are absorbed by the cadmium surrounding during the activation. It is defined by the thickness of the cadmium. Assuming a cutoff energy of $E_{\rm cutoff} = 0.5$ eV and neglecting the upper limit, the resonance integral is

$$\sigma_{\rm RI} = 2\alpha\sqrt{E_{\rm cutoff}} = 0.5\ {\rm eV}. \tag{18}$$

The ratio of the resonance integral to the thermal cross section [RI/th] can be written as

$$[{\rm RI/th}] = \frac{\sigma_{\rm RI}}{\sigma_{\rm th}} \approx 2\frac{E_{\rm th}}{E_{\rm cutoff}} \approx 0.45. \tag{19}$$

Using the pure $1/v$ extrapolation of the thermal value, which can be interpreted as the direct capture component, the contribution can be estimated as

$$[{\rm RI/th}]\sigma_{\rm th} = 0.45 \times 9.9\ {\rm b} \approx 4.5\ {\rm b}. \tag{20}$$

The remaining part, 193 b − 4.4 b = 188 b, originates from the resonances at higher energies and is by far dominating. Prior to our measurement, the thermal cross section of 160 barn could be expected to contribute up to 72 barn to the MACS cross section (based on an estimation similar to what is shown for the resonance to thermal contribution). Based on our new results, this contribution can be excluded and it is clear that only the resonant component will contribute significantly. This is important if future TOF experiments are capable of determining the resonance parameters of the ^{171}Tm(n, γ) cross section between 1 and 100 keV: if the DC can be neglected, the corresponding resonance yields can then directly be converted into a temperature-dependent MACS.

TABLE VI. Comparison of evaluated ^{171}Tm(n, γ) cross sections with our results. Data taken from [17] and the Atlas of Neutron Resonances, Resonance Parameters and Neutron Cross Sections [21].

Source	ROSFOND-2010	EAF-2010	Atlas	This work
$\sigma_{\rm th}$ (b)	160.1	160	60–190	**9.9 ± 0.9**
$\sigma_{\rm RI}$ (b)	449.6	468.6	325	**193 ± 14**

A comparison of our ^{171}Tm(n, γ) cross section values with those listed in evaluated data libraries is given in Table VI. The evaluations so far were largely based on a reactor activation experiment from 1971, which suggested a thermal cross section of 160^{+30}_{-100} b [6]. This experiment, however, suffered from large systematic uncertainties. First of all, the contributions from thermal and epithermal neutrons were not disentangled. This is extremely important, since the resonance integrals are large, hence the contribution from epithermal neutrons is not negligible. Second, the experiment was based on the long-term-irradiation of ^{170}Er and the measurement of the ^{172}Tm activity. Since there are several possible paths from ^{170}Er to ^{172}Tm (see Fig. 1), the contribution of the ^{171}Tm(n, γ) branch is not clear. In addition, the contribution from neutron captures on contaminants like ^{169}Tm is not discussed at all in [6]. Other experiments provide also hints at a much lower thermal capture cross section of only a few barn, which would be more in agreement with our result [5,20]. Unfortunately those results are very scarcely documented and not refereed. We therefore conclude that, to the best of our knowledge, the deviations from previous results and evaluations are largely due to undocumented systematic uncertainties of the previous measurements.

ACKNOWLEDGMENTS

We are very grateful for the excellent support by the entire team of the TRIGA reactor in Mainz. This work was partly supported by the BMBF Projects No. 05P12RFFN6 and No. 05P15RFFN1, the Helmholtz International Center for FAIR and HGS-HIRe, the DFG Project No. RE 3461/4-1, the European Research Council under the European Unions's Seventh Framework Programme (FP/2007-2013)/ERC Grant Agreement No. 615126 and project EC FP7-PEOPLE "NeutAndalus" with Grant Agreement No. 334315.

[1] R. Reifarth, C. Lederer, and F. Käppeler, J. Phys. G: Nucl. Phys. **41**, 053101 (2014).
[2] K. Takahashi and K. Yokoi, At. Data Nucl. Data Tables **36**, 375 (1987).
[3] R. Reifarth, R. Haight, M. Heil, M. Fowler, F. Käppeler, G. Miller, R. Rundberg, J. Ullmann, and J. Wilhelmy, Nucl. Phys. A **718**, 478 (2003).
[4] C. Guerrero, J. Lerendegui-Marco, C. Domingo-Pardo, A. Casanovas, R. Dressler, S. Halfon, S. Heinitz, N. Kivel, U. Köster, M. Paul *et al.*, *EPJ Web of Conferences* (EDP Sciences, 2017), Vol. 146, p. 01007.
[5] J. Gillette, Oak Ridge National Laboratory Report No. 4155, 1967 (unpublished), p. 15.
[6] K. Miyano, J. Phys. Soc. Jpn. **31**, 1304 (1971).
[7] K. Eberhardt and A. Kronenberg, Kerntechnik **65**, 5 (2000).
[8] G. Hampel, K. Eberhardt, and N. Trautmann, Atomwirtschaft **5**, 326 (2006).
[9] C. M. Baglin, Nucl. Data Sheets **96**, 399 (2002).

[10] M. Weigand, T. Heftrich, C. E. Düllmann, K. Eberhardt, S. Fiebiger, J. Glorius, K. Göbel, R. Haas, C. Langer, S. Lohse *et al.*, Phys. Rev. C **97**, 035803 (2018).
[11] I. Kajan, S. Heinitz, R. Dressler, P. Reichel, N. Kivel, and D. Schumann, Phys. Rev. C **98**, 055802 (2018).
[12] S. Heinitz, E. A. Maugeri, D. Schumann, R. Dressler, N. Kivel, C. Guerrero, U. Köster, M. Tessler, M. Paul, and S. Halfon, Radiochim. Acta **105**, 801 (2017).
[13] S.-C. Wu, Nucl. Data Sheets **91**, 1 (2000).
[14] B. Singh, Nucl. Data Sheets **130**, 21 (2015).
[15] X. H. and M. K., Nucl. Data Sheets **133**, 221 (2016).
[16] B. Singh, Nucl. Data Sheets **75**, 199 (1995).
[17] B. Pritychenko and S. Mughabghab, Nucl. Data Sheets **113**, 3120 (2012).
[18] R. Reifarth, C. Arlandini, M. Heil, F. Käppeler, P. Sedychev, A. Mengoni, M. Herman, T. Rauscher, R. Gallino, and C. Travaglio, Astrophys. J. **582**, 1251 (2003).
[19] R. Reifarth, F. Käppeler, F. Voss, K. Wisshak, R. Gallino, M. Pignatari, and O. Straniero, Astrophys. J. **614**, 363 (2004).
[20] J. Wilhelmy, E. Chamberlin, M. Dragowsky, G. Miller, P. Palmer, L. Pangualt, R. Rundberg, R. Haight, E. Seabury, J. Ullmann *et al.*, J. Nucl. Sci. Technol. **39**, 614 (2002).
[21] S. Mughabghab, *Atlas of Neutron Resonances, Resonance Parameters and Thermal Cross Sections, Z = 1–100* (Elsevier, New York, 2006).